

Chapter 15. Mesoscale Storm Systems

Karen S. Friedman

Office of Research and Applications, NOAA/NESDIS, Camp Springs, MD, USA

Paris W. Vachon

Canada Centre for Remote Sensing, Natural Resources Canada, Ottawa, Ontario, Canada

Kristina Katsaros

Atlantic Oceanographic and Meteorological Laboratory, Miami, FL, USA

15.1 Introduction

Mesoscale atmospheric storms, by influencing the near surface wind field, affect the sea surface roughness, which, in turn, can be imaged with synthetic aperture radar (SAR). In addition to increasing the understanding of typical low pressure systems that make their way across the oceans daily, SAR imagery has increased our knowledge of two particularly dangerous types of mesoscale storms: the polar mesoscale cyclone (PMC) and the tropical hurricane. The RADARSAT-1 ScanSAR Wide (SCW) mode swath width of 480 km to 520 km is wide enough to capture large portions of PMCs and hurricanes. SAR can penetrate clouds to provide images that can be used to infer the wind speed and storm structure at the ocean's surface with fine resolution (100 m for the SCW mode and 30 m for the standard mode of RADARSAT-1). Traditional visible and infrared weather sensors such as those on the NOAA Geostationary and Polar Operational Environmental Satellites, (GOES and POES, respectively), are limited to providing information on the top most level of the storm clouds. Other sensors, such as scatterometers (a microwave radar sensor that is used to measure wind speed and direction over the ocean surface) can also penetrate clouds, but are limited in their ability to observe localized wind events near the coast by its 15 km to 25 km resolution cell size.

SAR data have several potential roles in the monitoring and detection of storms over the ocean. First, ocean surface wind vectors can be estimated from the SAR image (see Chapter 13). Furthermore, the images provide visual evidence of convective cells, boundary layer rolls, wind shear zones, and storm centers (some of these are discussed in Chapter 14). The imagery also provides evidence of precipitation within these storms, which can be vital information if the storm is beyond the range of coastal Doppler radar (see Chapter 17). However, while SAR data is spatially rich, it can be temporally poor. A satellite based SAR must be programmed up to several days in advance to take data over a specified region. This makes it difficult to task coverage of infrequent and unpredictable storms, such as hurricanes, with more than a couple days' notice. For frequently occurring storms at high latitudes, such as PMCs, a system of staggered coverage can be set up months ahead of time. For example, for SCW at high latitudes, satellite revisit times of 1 to 2 days are possible, so that an area such as the Bering Sea can be completely imaged several times a week using multiple swaths. At lower latitudes, where hurricanes exist, the revisit time is 2 to 4 days. Also, the diameter of a hurricane is at least as wide as a SCW swath, so the chance of having a single pass cover the entire storm is low. For this reason, it is best to schedule passes over hurricanes once the predicted path is known, with minimum lead time.

15.2 Polar mesoscale cyclones

PMCs are a high latitude phenomenon, forming over the ocean in cold air masses poleward of the polar jet stream and associated frontal zones in both hemispheres. They are commonly found near ice/ocean or land/ocean boundaries where there is strong low-level baroclinicity due to differential heating of the atmospheric boundary layer over the water and ice/land region, or associated with the outflow of cold surface air from the continent (or ice covered ocean) over the water. PMCs most commonly occur during the fall, winter, and spring, form rapidly, and last only a couple of days. Several studies have examined PMCs with SAR [*Chunchuzov et al.*, 2000; *Sikora et al.*, 2000]. The size of PMCs (up to 1000 km, though often much smaller) allows a SCW swath to cover large portions of the storm in a single image.

PMCs pose a large risk to vessels in their path. Since PMCs are usually found in data poor regions (where few buoys or weather stations exist), there may be little or no warning of their existence and the imminent danger. For this reason, satellite data are important for detecting PMCs, especially by a sensor such as SAR that is not limited by clouds, because there often are multiple layers of clouds that mask low-level storm systems such as PMCs when imaged by passive sensors.

Friedman et al. [2000] demonstrated that by using SAR data in experimental forecasts involving PMCs, the U.S. National Weather Service improved its accuracy in the detection of such phenomena. Eventually it may be possible to classify the stages of PMC formation as seen in SAR, leading to better forecasts.

15.2.1 PMCs over the Bering Sea

PMCs in SAR imagery commonly take the appearance of either a hook or a spiral. In the Bering Sea, the hook-like variety is the most common [*Carlton*, 1985]. An example of a relatively small PMC observed on 16 January 2001 at 1821 UTC by RADARSAT-1 is shown in Figure 15.1a. As is typical of PMCs, it has formed off of the ice edge in the Western Bering Sea. The ice in the image is labeled ‘i’. The center of the PMC is a dark region of low backscatter at approximately 61°N, 179.5°E and is labeled ‘c’. Figure 15.1b is a GOES IR image taken 9 minutes later, at 1830 UTC, with 4-km resolution. Here the SAR coverage is outlined in a black box; the PMC is slightly but not obviously visible. The PMC sits in an air mass that is poleward of a much larger storm centered at 48°N, 165°W. The National Weather Service Marine Prediction’s Pacific Surface Analysis for 1800 UTC (Figure 15.1c) indicates that this large storm has a stationary front to its northwest. The PMC is on the north side of this front, though it was not shown on the analysis.

Wind rows in the atmosphere that affect sea surface roughness are found in the region labeled ‘r’ (Figure 15.1a) and indicate that the wind is blowing most likely perpendicular to the ice edge. Since this low pressure system rotates cyclonically, it is apparent that the wind is blowing from the ice and out to sea. The air over the ice is much colder than the air it interacts with over the ocean. The SAR image shows that the PMC is associated with a boundary that separates the cold air and high wind speeds to the north (higher backscatter) from a region of lower winds and warmer air to the south (lower backscatter). This boundary labeled ‘w’, forms the hook and arm shape of the PMC, and is most likely a wind shear boundary. The shear boundary is not straight, but is rather wave-like in appearance, and likely is developing instabilities. The region labeled ‘v’ highlights the SAR surface signature of boundary layer rolls. These roll signatures are not as strong as those in Figure 15.2. The region towards the

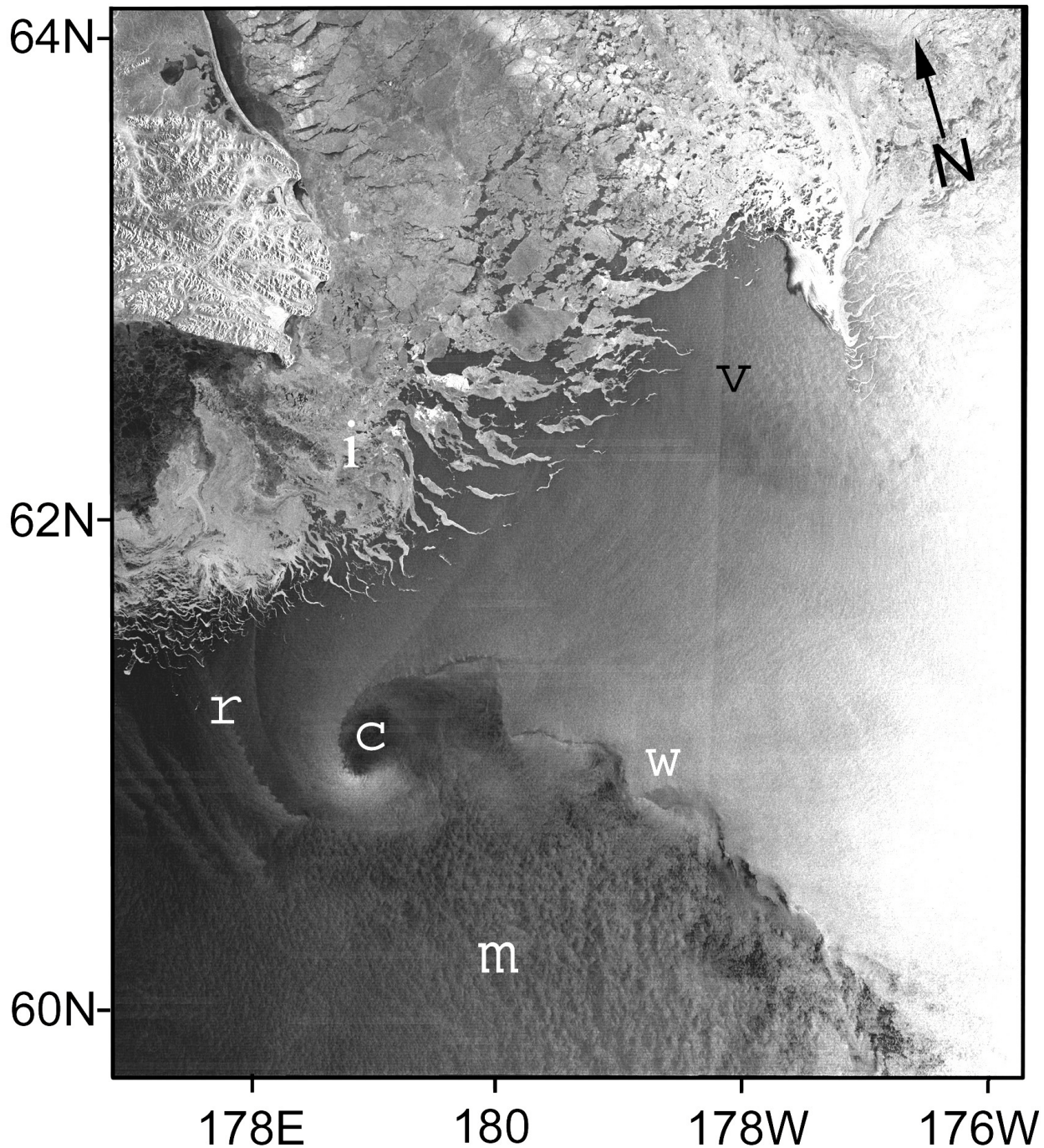


Figure 15.1a. RADARSAT-1 (C-band, HH) ScanSAR Wide image of a hook-like PMC over the Bering Sea acquired 16 January 2001 at 1821 UTC. Land in upper left is Cape Navarin, Russia. Ice covers the northern waters with finger-like extensions. The imaged area is 500 km wide. See text for explanation of labels. ©CSA 2001

bottom of the image, and south of the PMC's center, shows a mottled backscatter (labeled 'm') which is a signature of marine atmospheric boundary layer (MABL) cellular convection [Sikora *et al.*, 1995; 1997].

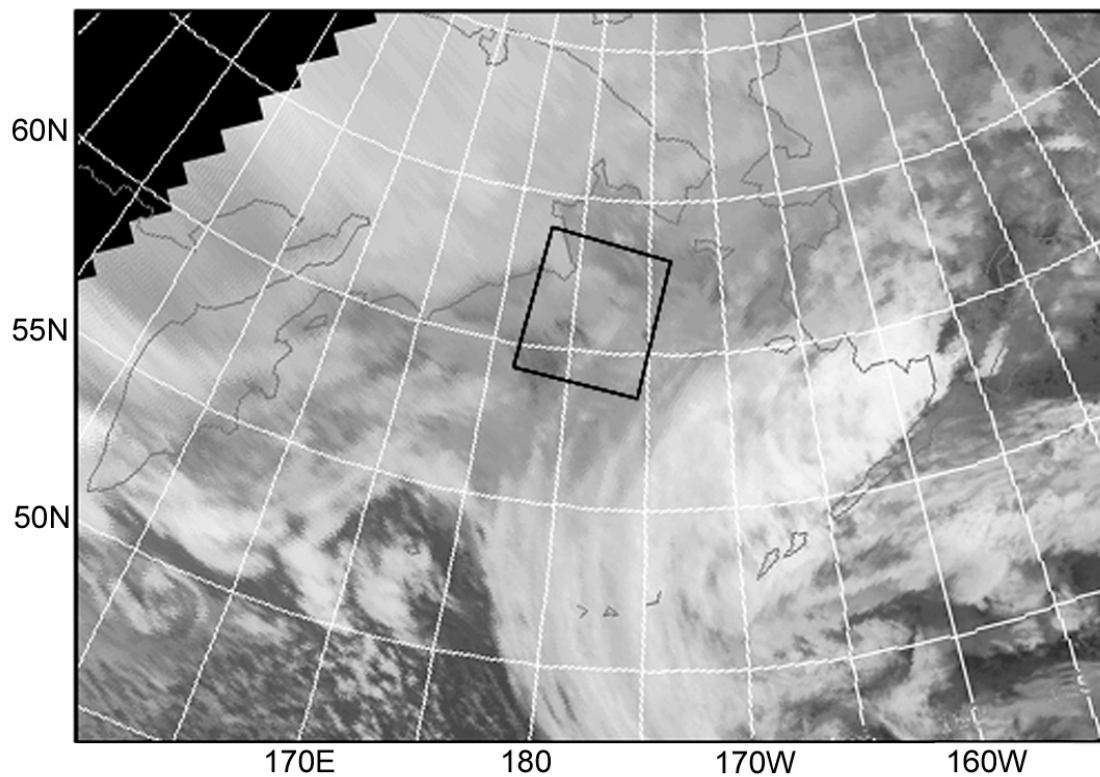


Figure 15.1b. NOAA GOES IR image of the Bearing Sea at 1830 UTC with the location of the SAR coverage.

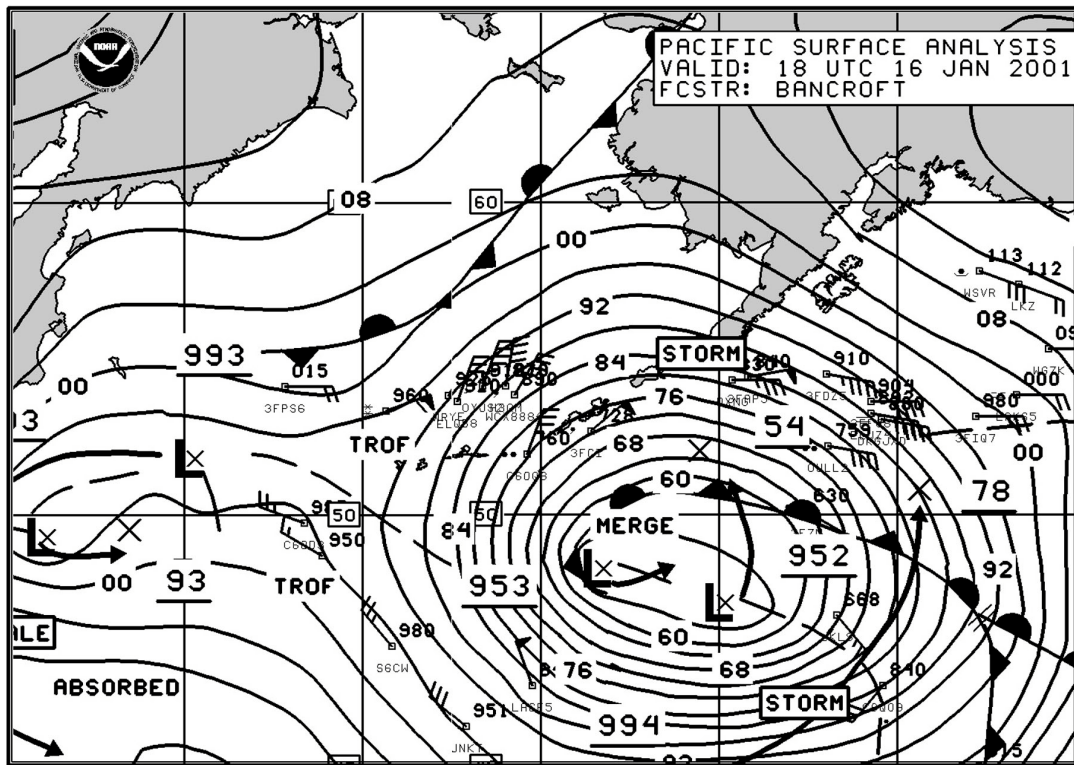


Figure 15.1c. NOAA National Weather Service Pacific Surface Analysis from 16 January 2001 at 1800 UTC.

15.2.2 PMC over the Labrador Sea

An example of a spiral-like PMC taken on 29 December 1997 at 2120 UTC by RADARSAT-1 is shown in Figure 15.2. The core of this well-developed PMC is close to the ice edge (labeled ‘i’) off Baffin Island. The interaction between an upper-level trough and the low-level baroclinicity near the ice edge is thought to have triggered the PMC. Organized deep convection probably contributed to its development and intensification.

The SAR image shows in detail the spiral-form structure of the surface wind field around the eye (the dark ellipsoid-shaped pattern) of the PMC. The convergence zone of the surface winds in the core of the PMC is characterized by several sharp wind field gradients that are revealed by the fine spatial resolution of the SCW image (labeled ‘w’).

According to a coastal weather station, a strong, cold westerly wind was blowing out over the coast, and sounding data indicate that the cold air mass was stably stratified over land. The cold air that was advected from Baffin Island to the warmer open water corresponds to the bright area visible in the left portion of the image. Downwind from the coast, the strong airflow becomes organized into spiral-form boundary layer rolls (labeled ‘v’) that become broader and farther apart as they move away from land. The horizontal roll spacing reaches 20 km at 300 km downwind. Cellular convection is evident to the northeast of the eye (top center of image labeled ‘m’). At the same time, the strong airflow that leaves the coast appears to be stable (the bright area southwest of the eye), but quickly destabilizes with downwind distance from the coast, probably because of strong heat fluxes from the warmer ocean.

15.3 Hurricanes

Hurricanes originate at low latitudes in the Atlantic and Pacific Oceans, the Gulf of Mexico, and the Caribbean Sea. In the Atlantic Basin (including the Gulf of Mexico and Caribbean Sea), they occur between approximately June and November, and they form in the eastern Pacific Ocean approximately within the same time period. A tropical cyclone can form when a pre-existing disturbance exists (unorganized mass of thunderstorms with very little, if any, organized wind circulation) along with warm ocean temperatures, light upper level winds, and low wind shear. When the tropical cyclone reaches a sustained wind speed of 33 m s^{-1} (64 knots) it is classified as a hurricane. Hurricanes have an eye around which the winds blow in a cyclonic spiral pattern. The eye is relatively calm and may be between 30 km and 50 km in diameter. Hurricanes vary in size but their powerful winds can extend more than 500 km out from the eye. Hurricane-like cyclones are created around the world from similar conditions, but are known by other names such as typhoon in the Western North Pacific, and tropical cyclone in the Indian Ocean and Western South Pacific. In-situ and ground-based Doppler weather radar data are quite common when hurricanes are within a few hundred kilometers of U.S. coastal regions, but outside of this range, data are sparse except from satellites. SAR has the unique ability to provide very fine resolution observations of the wind signatures at the ocean surface within a hurricane, which in the future may be important inputs to forecast and landfall prediction models. Hurricane winds, rain, and storm surges threaten land, property, and personal safety. Improving the models will lead to better predictions. There have been several case studies of SAR imaging of hurricanes [Vachon and Katsaros, 1999; Katsaros *et al.*, 2000; Friedman and Li, 2000].

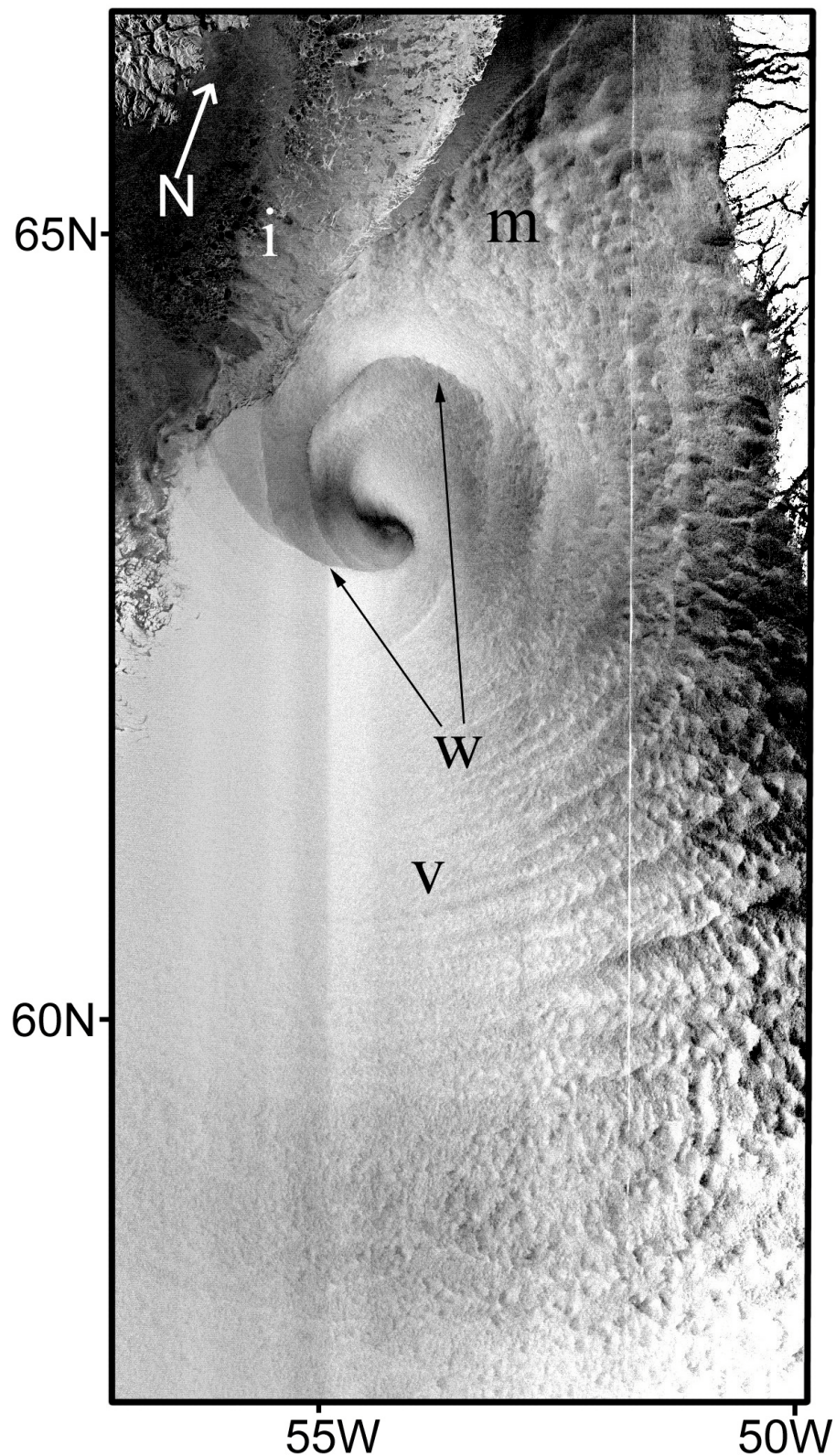


Figure 15.2. RADARSAT-1 (C-band, HH) ScanSAR Wide image of a spiral-like PMC in the Labrador Sea. The imaged area is 500 km wide. See text for explanation of labels. ©CSA 1997

Mesoscale Storm Systems

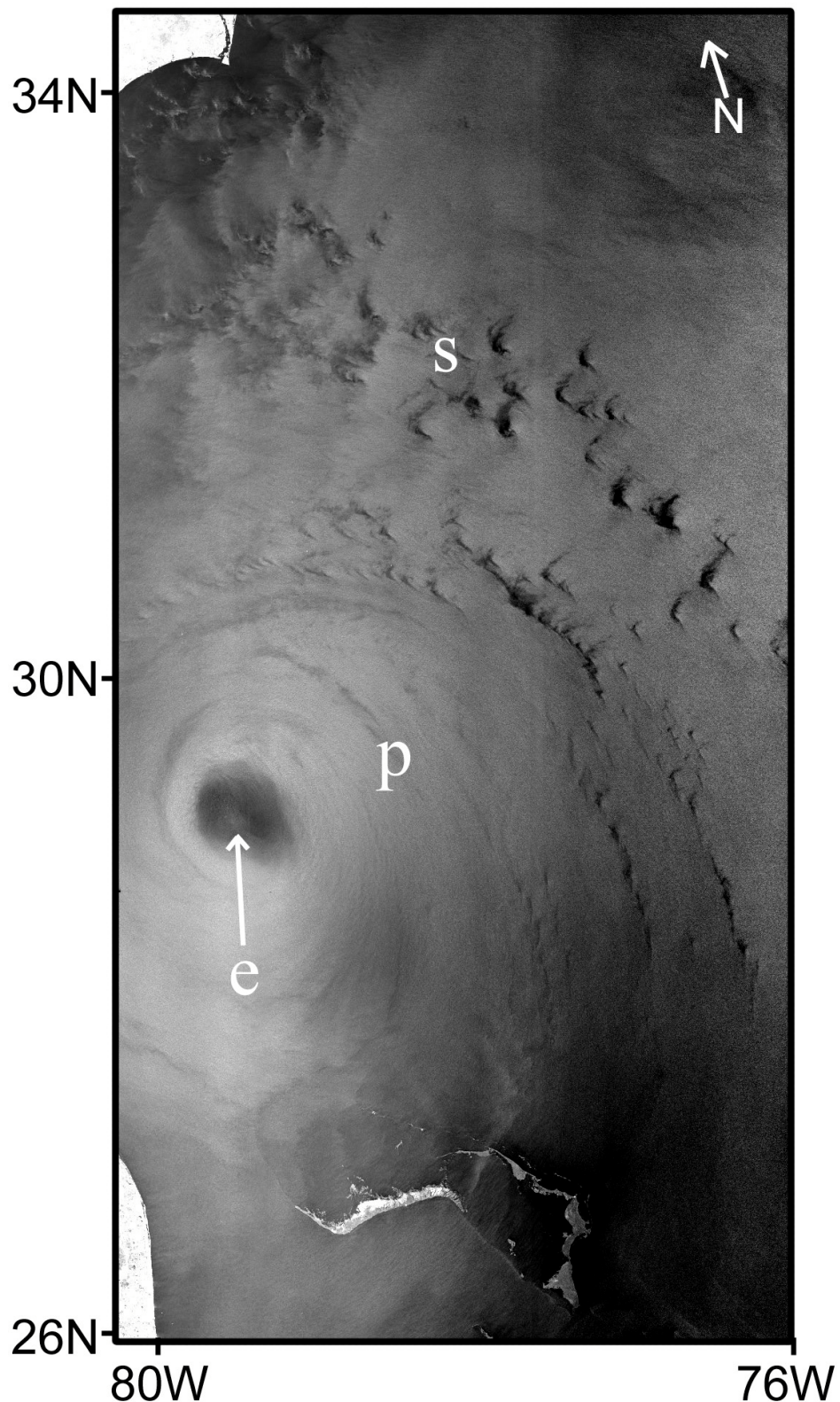


Figure 15.3a. RADARSAT-1 (C-band, HH) ScanSAR Wide image of Hurricane *Floyd* acquired 15 September 1999 at 1108 UTC. The imaged area is 500 km wide. Land in upper left is Cape Fear, North Carolina, at the bottom left is Florida, and islands at bottom center are the Bahamas. See text for explanation of labels. ©CSA 1999

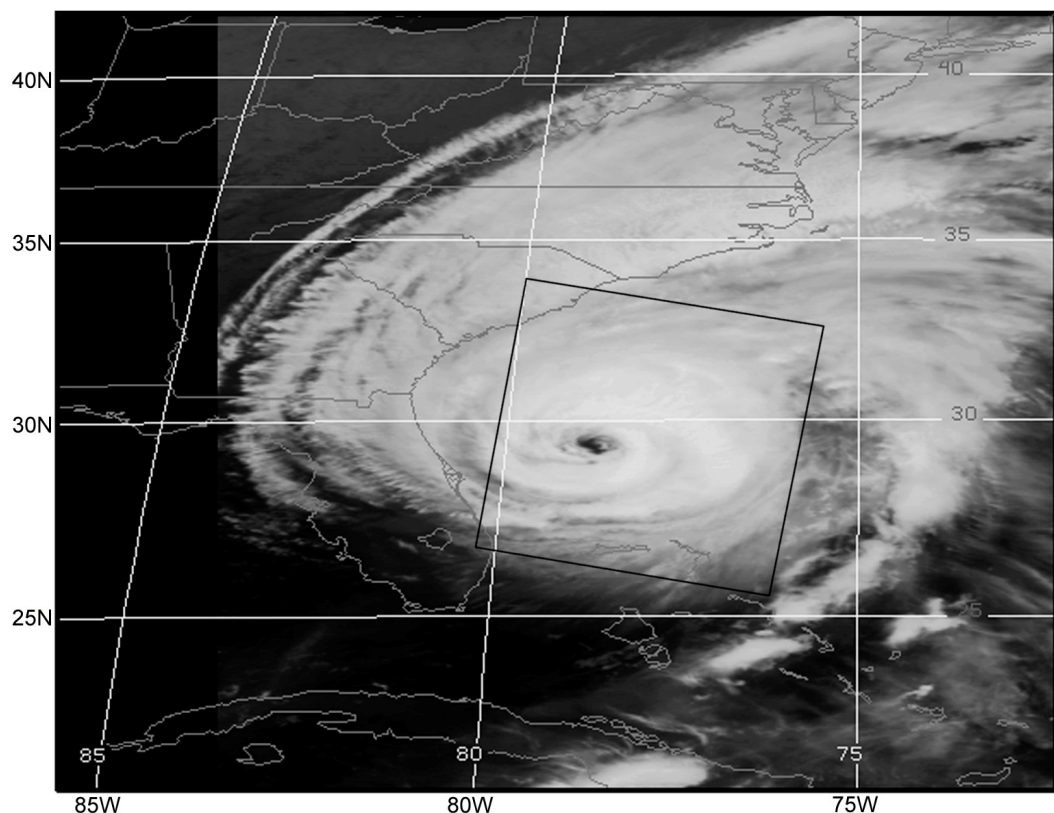


Figure 15.3b. NOAA GOES IR image of Hurricane *Floyd* at 1115 UTC with the location of the SAR coverage

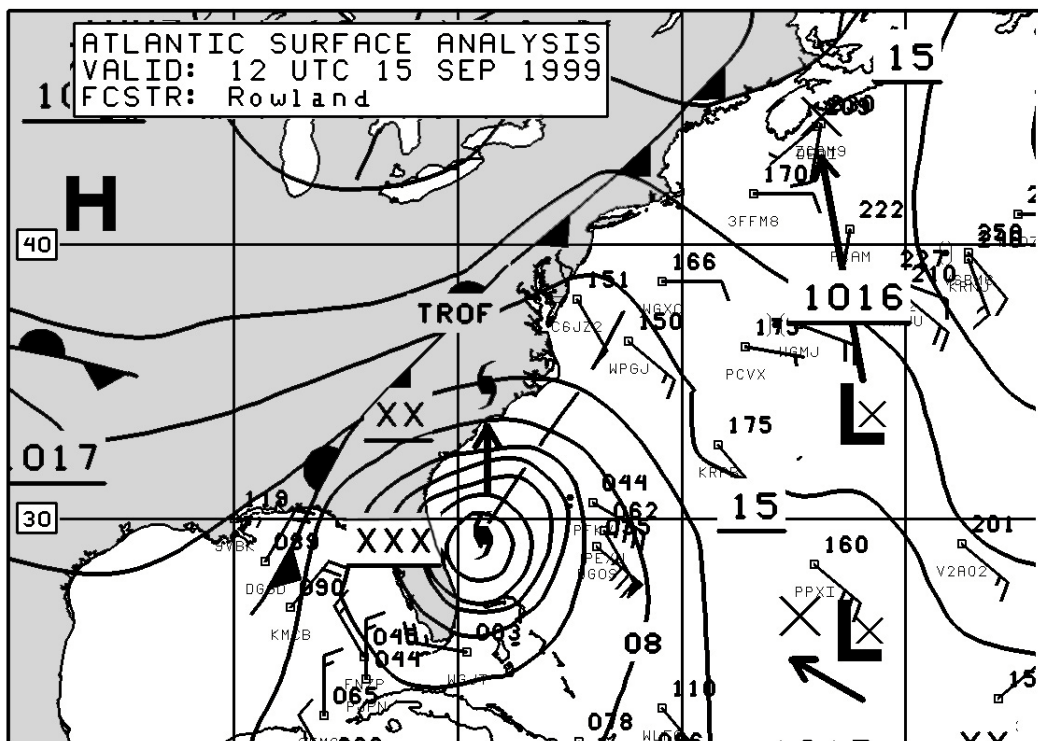


Figure 15.3c. NOAA National Weather Service Atlantic Surface Analysis from 15 September 1999 at 1200 UTC.

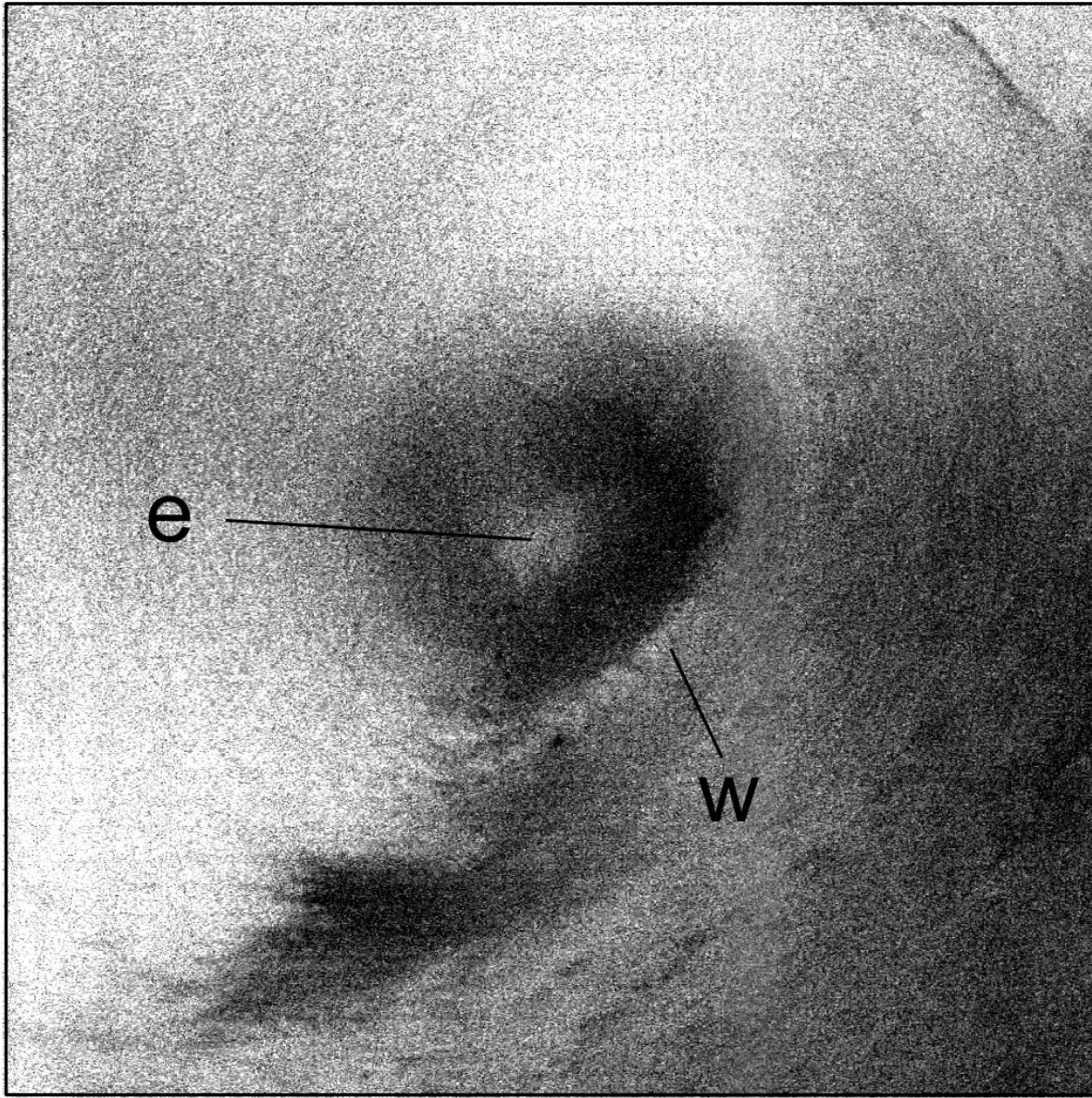


Figure 15.4. RADARSAT-1 (C-band, HH) SAR ScanSAR Wide sub-image (100 km) of the eye of Hurricane Dalila (in the Pacific) acquired 26 July 2001 at 0124 UTC. See text for explanation of labels. ©CSA 2001.

15.3.1 Hurricane Floyd

Figure 15.3a shows a SCW image of Hurricane Floyd off the U.S. East Coast on 15 September 1999 at 1108 UTC. The image clearly shows the relatively calm eye of the hurricane with a diameter of about 50 km. The storm covers the full extent of the 500-km SCW swath. The SAR image area is indicated by the box in Figure 15.3b (the GOES IR image taken 7 minutes later). The SAR image covers only a portion of the hurricane's extent as measured by the associated storm clouds. On the surface analysis at 1200 UTC (Figure 15.3c) high winds associated with the hurricane and also a stationary front to its Northwest can also be seen. Readily visible in the SAR are dark, banded features that are associated with intense

precipitation (labeled ‘p’). Raincells in SAR imagery are discussed in Chapter 17. Several pre-hurricane squall lines composed of a series of convective cells are visible to the north of the eye (labeled ‘s’). The image brightness around the eye is modulated by the changing wind direction relative to the SAR look direction (See Chapter 13). In the center of the hurricane’s eye there exists a small region of high backscatter (labeled ‘e’). This phenomenon has been seen in several RADARSAT-1 images of hurricane eyes. Another example is shown in Figure 15.4 of Hurricane Dalila, labeled ‘e’ also.

Another interesting phenomenon, seen in some of the SAR images of hurricane eyes, are the wave patterns around the eye wall. This is shown in Figure 15.4 of Hurricane Dalila and labeled ‘w’. It is possible that these are caused by atmospheric instability waves.

Besides Floyd and Dalia, there are many SAR images of hurricanes obtained by RADARSAT-1 during the 1998, 1999, 2000 and 2001 hurricane seasons. The images have revealed several interesting features that were not well known earlier, including the ubiquitous presence of boundary layer secondary flow phenomena such as roll vortices—the effects of small intense vortices on the eye wall extending high wind bursts into the eye area and the patterns in the wind field along the eye. The usefulness of SAR imaging in hurricane research is just beginning to be understood.

15.4 References

- Carleton, A. M., 1985: Satellite climatological aspects of the “polar low” and “instant occlusion.” *Tellus*, **37A**, 433–450.
- Chunchuzov, I., P. W. Vachon, and B. Ramsay, 2000: Detection and characterization of polar mesoscale cyclones in RADARSAT synthetic aperture radar images of the Labrador Sea. *Can. J. Remote Sens.*, **26**, 213–230.
- Friedman, K. S., and X. Li, 2000: Monitoring hurricanes over the ocean with wide swath SAR. *Johns Hopkins APL Tech. Dig.*, **21**, 80–85.
- , T. D. Sikora, W. G. Pichel, P. Clemente-Colón, and G. Hufford, 2001: Using spaceborne synthetic aperture radar to improve marine surface analyses. *Wea. Forecasting*, **16**, 270–276.
- Katsaros, K., P. Vachon, P. Black, P. Dodge, and E. Uhlhorn, 2000: Wind fields from SAR: Could they improve our understanding of storm dynamics? *Johns Hopkins APL Tech. Dig.*, **21**, 86–93.
- , P. W. Vachon, W. T. Liu, and P. G. Black, 2002: Microwave remote sensing of tropical cyclones from space. *J. Oceanogr.*, **58**, 137–151.
- Sikora, T. D., G. S. Young, R. C. Beal, and J. B. Edson, 1995: Use of ERS-1 synthetic aperture radar imagery of the sea surface in detecting the presence and structure of the convective marine atmospheric boundary layer. *Mon. Wea. Rev.*, **123**, 3623–3632.
- Sikora, T. D., G. S. Young, H. N. Shirer, and R. D. Chapman, 1997: Estimating convective atmospheric boundary layer depth from microwave radar imagery of the sea surface. *J. Appl. Meteor.*, **36**, 833–845.
- Sikora, T. D., K. S. Friedman, W. G. Pichel, and P. Clemente-Colón, 2000: Synthetic aperture radar as a tool for investigating polar mesoscale cyclones. *Wea. Forecasting*, **15**, 745–758.
- Vachon, P. W., and K. Katsaros, 1999: RADARSAT SAR provides images of atmospheric cyclones. *Backscatter*, **10**, 14–19.